



## Deployment simulation of foldable origami membrane structures

Jianguo Cai <sup>a,\*</sup>, Zheng Ren <sup>b</sup>, Yifan Ding <sup>b</sup>, Xiaowei Deng <sup>c</sup>, Yixiang Xu <sup>d</sup>, Jian Feng <sup>e</sup>

<sup>a</sup> Key Laboratory of C & PC Structures of Ministry of Education, National Prestress Engineering Research Center, Southeast University, Nanjing 210096, China

<sup>b</sup> School of Civil Engineering, Southeast University, Nanjing 210096, China

<sup>c</sup> Department of Civil Engineering, The University of Hong Kong, Hong Kong

<sup>d</sup> Department of Civil Engineering, University of Strathclyde, UK

<sup>e</sup> National Prestress Engineering Research Center, Southeast University, Nanjing 210096, China



### ARTICLE INFO

#### Article history:

Received 1 October 2016

Received in revised form 12 December 2016

Accepted 2 April 2017

Available online 5 April 2017

#### Keywords:

Deployable structure

Membrane

Unfolding

Origami

### ABSTRACT

In recent years, with the development of the space structures, thin film reflector structures have the feature of lightweight, high compact ratio, easy to fold and unfold and so on. Its form has received wide attention from researchers and a broad application prospect. In this paper, the nonlinear finite element software ABAQUS was used to carry out the numerical simulation of the deployment of membrane structures based on Miura-ori, by taking advantage of the variable Poisson's ratio model to revise the stress distribution of membrane elements. Then the uniaxial tension tests were carried out to study the material properties of the polyimide film. The effective elastic modulus was used to simulate the crease of the membrane. The deployment of a membrane structure based on Miura origami pattern was studied. Moreover, effects of some parameters, such as the number of loading nodes and the loading rate on the numerical results were discussed.

© 2017 Elsevier Masson SAS. All rights reserved.

## 1. Introduction

There is currently much interest in the use of ultra-light space structures, especially the gossamer structures [1,2]. Thin-film membranes stretched in tension are found to meet the requirements of future gossamer spacecraft [3–5]. If the size of the gossamer spacecraft is large, it is envisaged that the membrane structure will be folded for packaging purpose. The folding process can be realized based on the concept of origami.

Origami, a traditional Asian paper craft, has been proved as a valuable tool to develop various deployable and foldable structures [6–9]. Miura-ori, which is a well-known rigid origami structure utilized in the packaging of deployable solar panels for use in space or in the folding of maps [10]. Every node of Miura-ori has four creases/fold lines, three mountain fold lines and one valley fold line or three valley fold lines and one mountain fold line. The deployment of the Miura-ori is given in Fig. 1. The Miura-ori crease pattern can also be used to pack and deploy the membrane [11,12]. Therefore, the Miura-ori membrane structure is selected as the objective for this study.

The membrane structure is prone to wrinkling [13–17]. The existence of wrinkled regions may have adverse influence on the deployment of a membrane structure. Tension field theory, was firstly proposed by Wagner [18] to consider the wrinkled membranes. Then Reissner [19] developed a numerical method to obtain a non-compression solution for isotropic membranes based on the tension field theory. However, the tension field theory cannot give the amplitude, wavelength and numbers of wrinkles. Therefore the bifurcation analysis based on shell elements was introduced [14,20]. But the results are dependent on the element mesh, and the numerical simulation is hard to converge [21]. Stein and Hedgepeth [22] proposed a variable Poisson's ratio model to study the wrinkling of membranes. Then Miller and Hedgepeth [23] further developed a new algorithm for the numerical simulation. Recently, Patil et al. [24,25] studied the wrinkling of non-uniform membranes with non-uniform thickness.

Creases, or folding lines, of an origami pattern may also have great effects on the mechanical behavior and deployment performance of foldable membrane structures. Gough et al. [26] carried out experimentally and numerically studies on a square creased membrane. Woo et al. [27] studied the effective modulus of creased membranes based on the geometrically and materially finite element simulation of the whole process of creasing. The results were also compared with experiments. Then Woo and Jenkins [28] studied the wrinkling of a creased square membrane under different corner loads. Moreover, they also studied the effects of

\* Corresponding author.

E-mail addresses: [j.cai@seu.edu.cn](mailto:j.cai@seu.edu.cn) (J. Cai), [1175455218@qq.com](mailto:1175455218@qq.com) (Z. Ren), [dingnewstart@163.com](mailto:dingnewstart@163.com) (Y. Ding), [xwdeng@hku.hk](mailto:xwdeng@hku.hk) (X. Deng), [yixiang.xu@strath.ac.uk](mailto:yixiang.xu@strath.ac.uk) (Y. Xu), [fengjian@seu.edu.cn](mailto:fengjian@seu.edu.cn) (J. Feng).

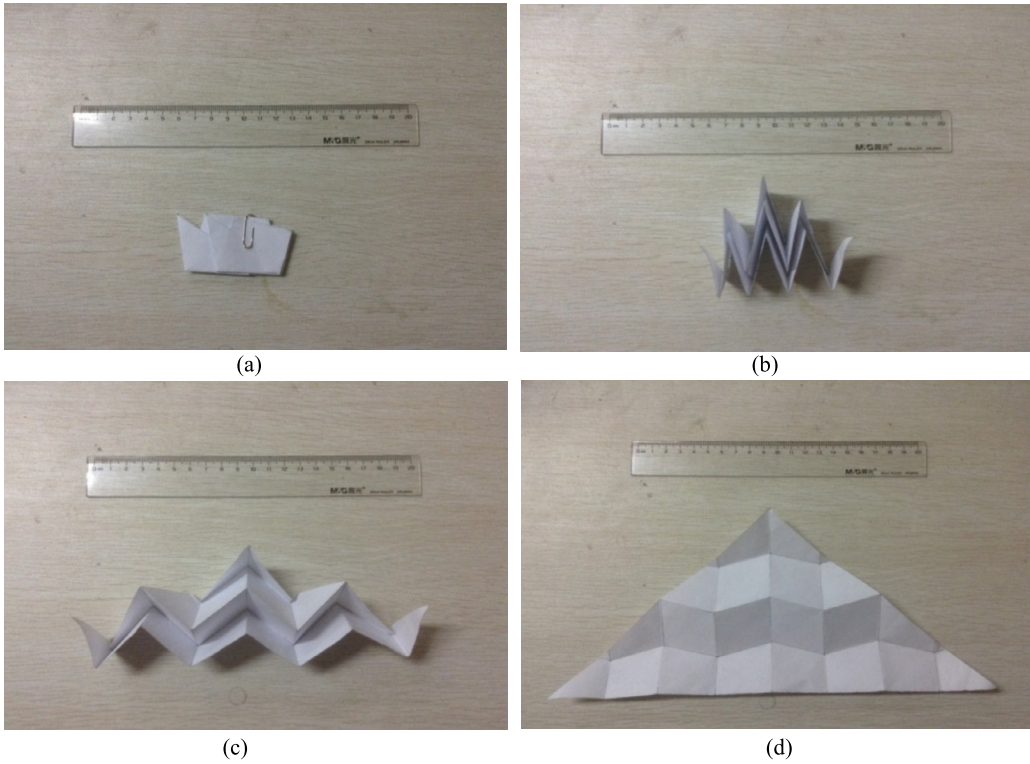


**Fig. 1.** Deployment of Miura-ori.

the membrane thickness [29] and the crease orientation [30], deployment angle and load ratio [31]. Wang et al. [32] investigated the shear performance of a rectangular membrane considering the wrinkling and creases.

So far most of the previous studies only focus on the membranes with single or simple creases. Papa and Pellegrino [33] studied the mechanics of a systematically creased square membrane with the Miura-ori pattern. However, to use the thin shell method for creased membranes, the initial imperfections should be quantitatively introduced to the numerical model [34]. In addition, to obtain better results in deformation, the refined element meshes lead to a large number of shell elements. In this paper, the membrane element with the variable Poisson's ratio model is used to model the wrinkling of membranes and the effective crease modulus of thin films, which are obtained from experiments, is used to consider the creases of Miura-ori pattern. Moreover, effects of the number of loading nodes, the time of the loadings and loading positions of the membrane on the deployment performance are also discussed.

## 2. Modelling of membrane wrinkling

The variable Poisson's ratio model will be introduced in this section to model the wrinkling of membranes. The stress-strain relationship within a statically determinant region of uniaxial stress that could be an approximation to the state of stress within a wrinkled portion of the membrane should be constructed. In a taut region, the stresses and strains are related according to the usual plane stress elastic equations for isotropic and elastic solids. However, within a wrinkled region, the usual elastic equations don't apply. Instead the assumption of negligible bending stress in the membrane yields the stress

$$\sigma_1 = E\varepsilon_1, \quad \sigma_2 = 0, \quad (1)$$

where  $\sigma$  is the stress,  $\varepsilon$  is the strain,  $E$  is the Young's modulus, the subscript 1 and 2 are the directions parallel and perpendicular to

the wrinkles, respectively. For the purpose of numerical analysis, it is desirable to express the stress in terms of the strains in the matrix form as

$$\{\sigma\} = [D]\{\varepsilon\}, \quad (2)$$

where

$$\{\sigma\} = \{ \sigma_x \ \sigma_y \ \tau_{xy} \}^T \quad \text{and} \quad \{\varepsilon\} = \{ \varepsilon_x \ \varepsilon_y \ \gamma_{xy} \}^T. \quad (3)$$

Normally, the matrix  $[D]$  can be written as

$$[D] = \frac{E}{1-\lambda^2} \begin{bmatrix} 1 & \lambda & 0 \\ \lambda & 1 & 0 \\ 0 & 0 & (1-\lambda)/2 \end{bmatrix}, \quad (4)$$

where the "variable Poisson's ratio"  $\lambda$  varies from point to point within the wrinkled region so that  $[D]$  is not a constant matrix. However, because of the presence of the term  $1/(1-\lambda^2)$ ,  $[D]$  is not suitable for numerical implementation within the wrinkled region where  $\lambda = 1$ . Hence another representation for  $[D]$  is given by Miller and Hedgepath [19] as

$$[D] = \frac{E}{4} \begin{bmatrix} 2(1+P) & 0 & Q \\ 0 & 2(1-P) & Q \\ Q & Q & 1 \end{bmatrix}, \quad (5)$$

where  $P = (\varepsilon_x - \varepsilon_y)/(\varepsilon_1 - \varepsilon_2)$  and  $Q = \gamma_{xy}/(\varepsilon_1 - \varepsilon_2)$ . No singularities of the matrix are observed for any value of  $P$  and  $Q$  between 0 and 1, and hence this numerical representation of  $[D]$  has no difficulties.

The iterative membrane properties (IMP) method, which uses the variable Poisson's ratio theory to recursively modify the properties of membrane elements until all the compressive stresses disappear when tensioned, is implemented based on the software ABAQUS [13,28]. Then a user-defined material ABAQUS/Explicit subroutine (VUMAT) is written to incorporate the wrinkling effects into the membrane. In practice, the constitutive matrix  $[D]$

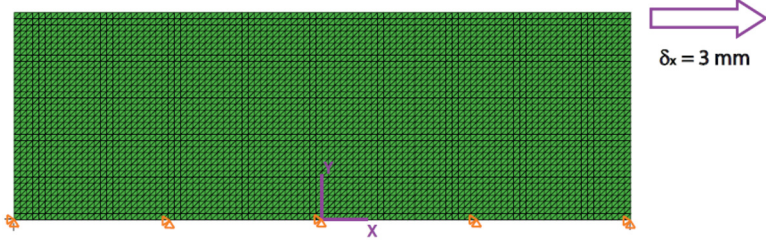
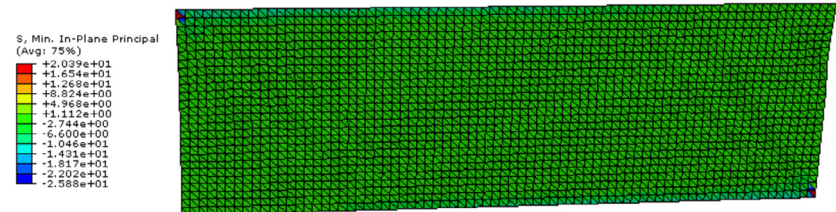


**Fig. 2.** A rectangular membrane under simple shear.

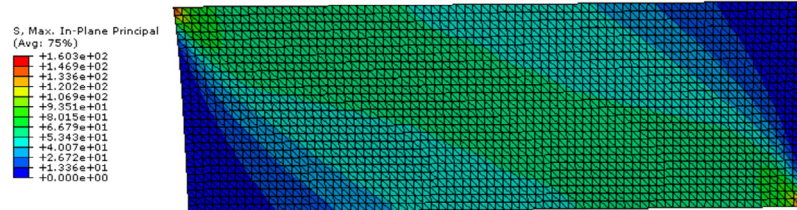


(a) Major principal stress (MPa)

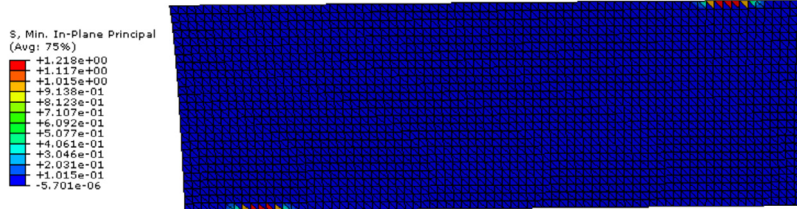


(b) Minor principal stress (MPa)

**Fig. 3.** Results of membrane elements.



(a) Major principal stress (MPa)



(b) Minor principal stress (MPa)

**Fig. 4.** Results of membrane elements with variable Poisson's ratio.

is updated at each increment according to different status of individual membrane element. A test case, which involves a rectangular membrane under shearing loads, is chosen as an example to validate the subroutine. The length of the rectangular membrane is 300 mm and the width is 180 mm. The Young's modulus is 4623.2 MPa with a Poisson's ratio 0.34, and the thickness is 0.025 mm. The membrane was modeled with 3-node, fully integrated triangular membrane elements (M3D3). All translations of the bottom edge nodes were fully constrained. As shown in Fig. 2,

the shear load was applied by prescribing a horizontal shear displacement of the top edge where the upper edge nodes moved by 3 mm in the length-wise direction while all other translations were constrained.

The stress distribution at the end of the horizontal displacement is illustrated by means of contour plots in Figs. 3 and 4. Fig. 3 shows the results with membrane elements only. When the variable Poisson's ratio model is used, the results are given in Fig. 4. It can be found that the membrane finite element model using

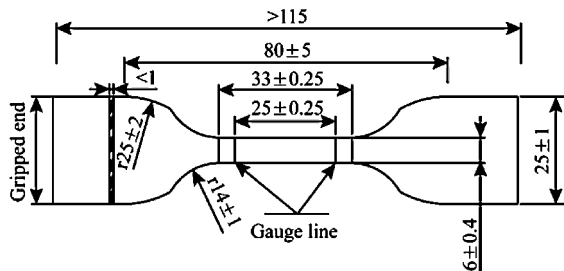


**Fig. 5.** Size of the membrane specimen (mm).

the VUMAT subroutine has succeeded in eliminating all negative stress, as illustrated by the minor stress distribution being approximately non-negative everywhere. In addition, the high stresses at the top-left and bottom-right corners indicate two areas of stress concentration.

### 3. Experimental tests of material behaviors

#### 3.1. Mechanical properties of membranes

The experimental set-up and protocol for the material behavior study was based on the design code. The size of the specimen is shown in Fig. 5. The miniature materials tester (CMT4503) was used to conduct the study.

Instead of the conventional measuring method, digital image correlation (DIC) was used in the test. This is because the conventional strain gauge cannot measure when the ultimate strain of thin film exceeds the range of strain gauge. The DIC method with the advantages of non-destruction, non-contact, high precision is widely used in research of mechanical and engineering tests. It is a method based on the principle of binocular stereo vision and the technology of digital image correlative matching. The displace-

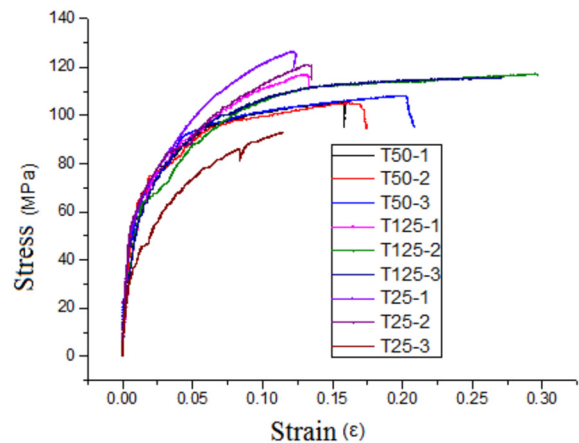


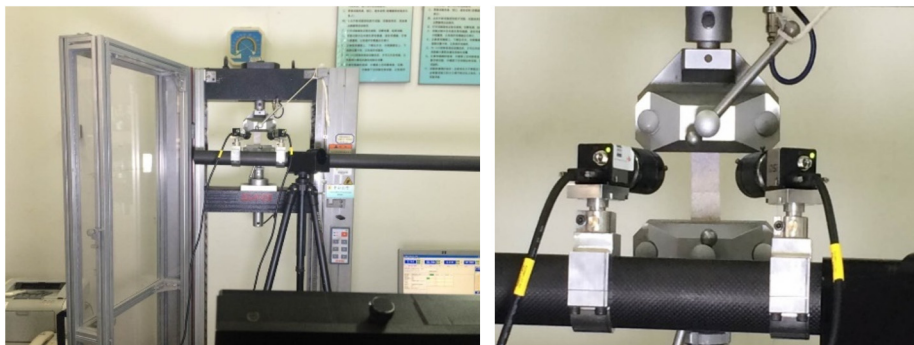
**Fig. 8.** Stress-strain curves.

**Table 1**  
Mechanical property of polyimide thin film 6051.

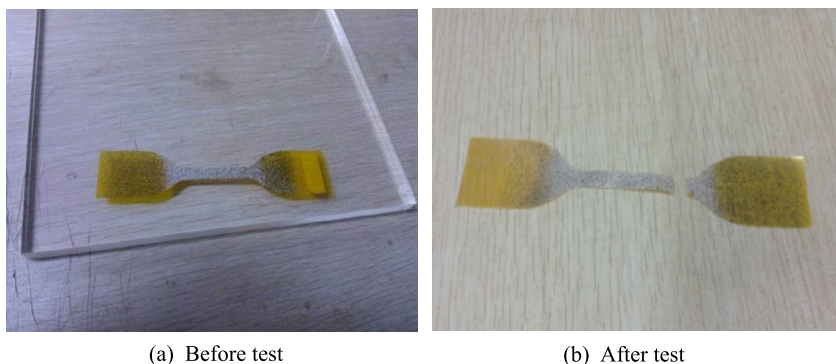
Thickness	25 μm	50 μm	125 μm
Young's modulus $E$ /MPa	4623.2	4300.8	3647.8
Yield strength $\sigma_y$ /MPa	60.01	59.66	59.76
Yield strain $\varepsilon_y$	0.00995	0.00973	0.01336

ment field is fitted using least square method, and the strain field can be obtained after smoothing and differential processing. Material test measurement set-up and test specimens are shown in Figs. 6 and 7.

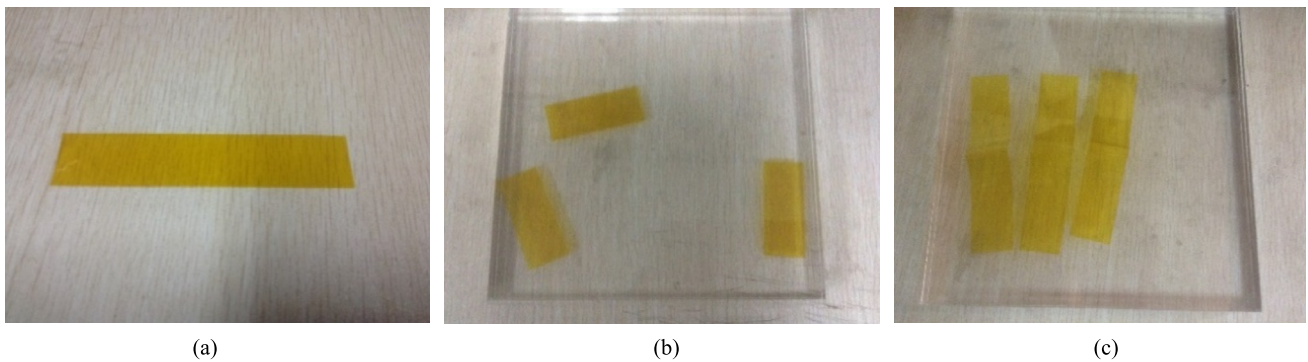
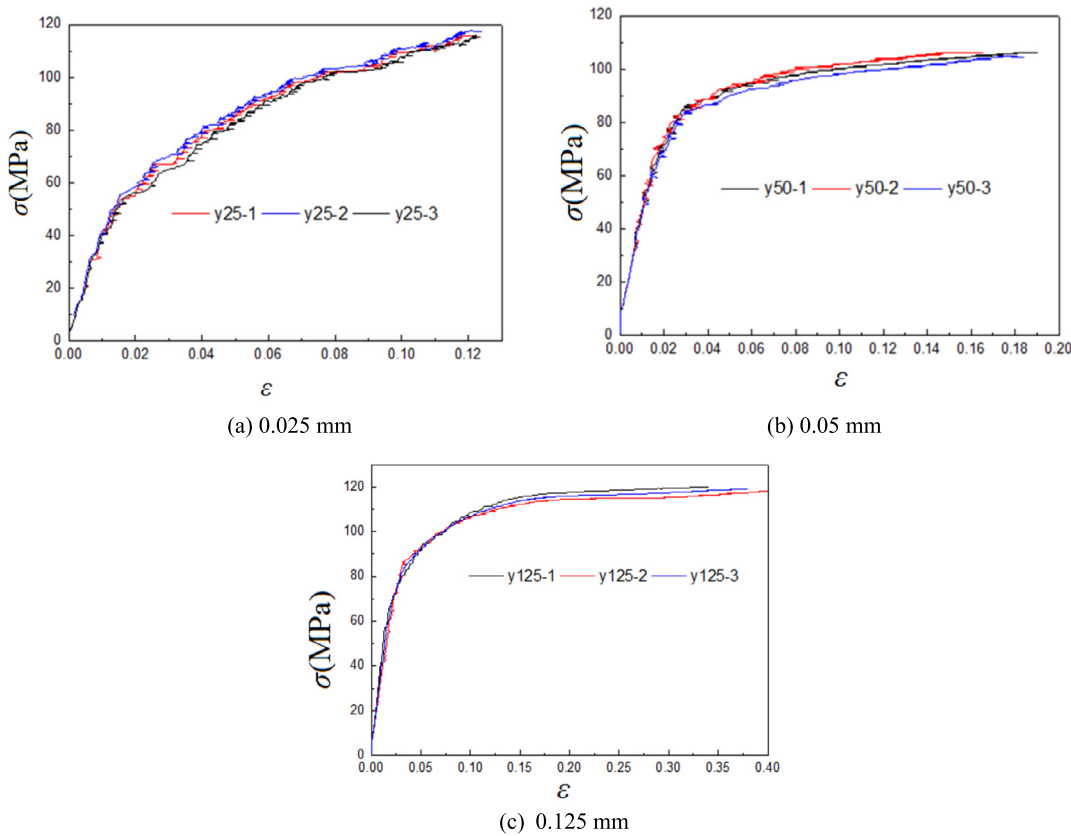
thicknesses of the membrane specimens were tested: 25 μm, 50 μm and 125 μm, three samples in each, giving an stress strain curves as shown in Fig. 8. Table 1 shows the average mechanical parameters of materials.



**Fig. 6.** Experimental set-up.



**Fig. 7.** Test specimens.

**Fig. 9.** The process to obtain the creased membranes.**Fig. 10.** Stress–strain curves for creased membranes.

### 3.2. Mechanical properties of creased membranes

The creases of the membrane can be seen as inelastic deformation. Then the linear mechanical property given in table cannot be used for the region of creases. The effective modulus method is used in this paper. The present experimental work of effective modulus followed from previous work. In the present case, specimens used for the experiment were cut out from polyimide thin film 6051 membrane. As shown in Fig. 9, a rectangle of the size 125 mm × 25 mm was marked on the sheet of polyimide thin film 6051 by use of a template and specimens were cut out by using a razor cutter. Care was taken to obtain regular geometry for each specimen. Specimens were lightly folded and placed between the two glass panels. The strain–stress curves of every specimens are given in Fig. 10. The test results of the effective modulus are shown in Table 2.

**Table 2**  
The effective modulus of creased membranes.

Thickness	Effective modulus
0.025 mm	3592.8 MPa
0.05 mm	3936.2 MPa
0.125 mm	3161.3 MPa

### 4. Deployment simulation of Miura-ori membrane

A Miura-ori membrane as shown in Fig. 11 is chosen as an numerical example. The size of the membrane is given in Fig. 11(a). The thickness of the membrane is 0.025 mm. For the numerical study, the part besides the crease as shown in Fig. 11(b) are assumed to have the effective modulus of creased membranes, which is given in Table 2. As for the rest region, the elastic modulus ob-

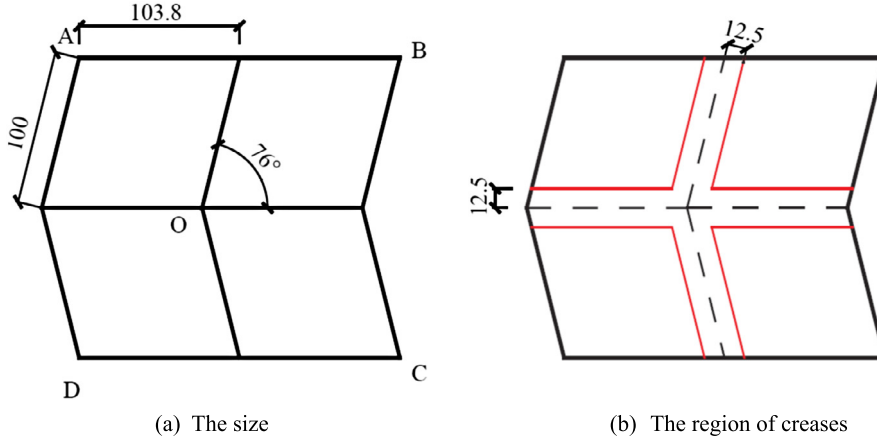


**Fig. 11.** The geometric parameters of the Miura-ori element (mm).

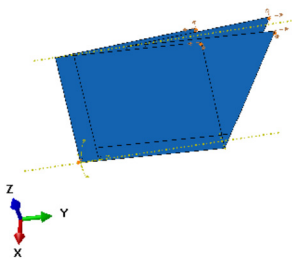


**Fig. 12.** The initial configuration of the membrane.

tained by material performance test, which is given in [Table 1](#), was adopted.

The deployment process from the folded configuration to the deployed configuration was numerically studied by ABAQUS. The initial configuration of the membrane is shown in [Fig. 12](#). The co-

**Table 3**  
The magnitude of applied nodal velocity (mm/s).

Node number	A	B	C	D
X-axis	-882.98	-882.98	882.98	882.98
Y-axis	-1533.48	26.18	26.18	-1533.48
Z-axis	0	0	0	0

ordinate is also given in this figure. The node O was fixed in all directions. The four corner nodes A, B, C, D were fixed in the z direction. And the loads were applied on these four nodes to active the deployment. Moreover, the nodal velocity was chosen as the nodal load in this study. The magnitudes of applied nodal velocity are given in [Table 3](#). The deployment process lasted 0.1 s.

The deployment of Miura-ori membrane from the initial folded state to the fully open state is shown in [Fig. 13](#). To study the deployment behavior, two indexes, the smoothness index and the

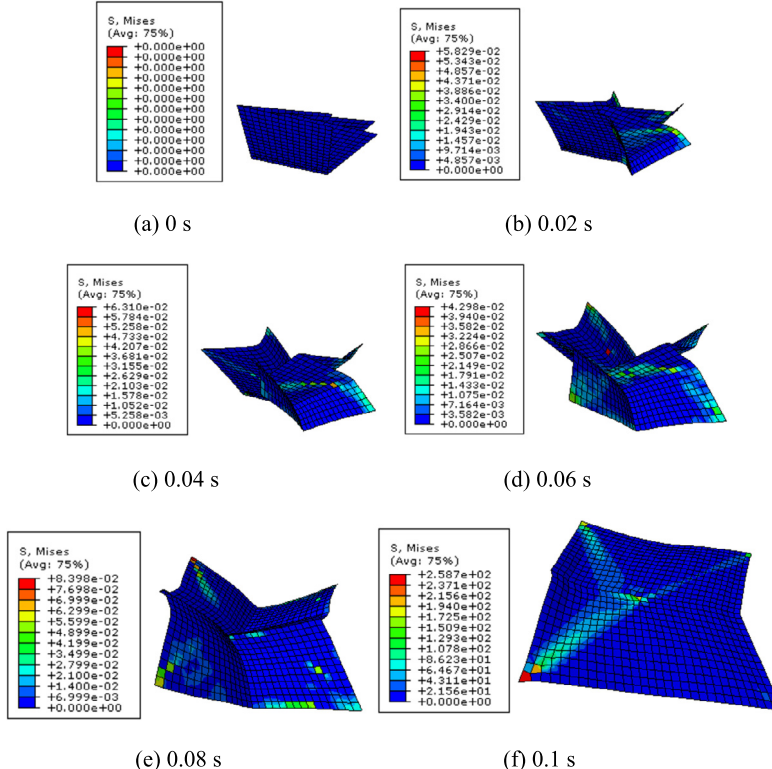


**Fig. 13.** The deployment of Miura-ori membrane (MPa).

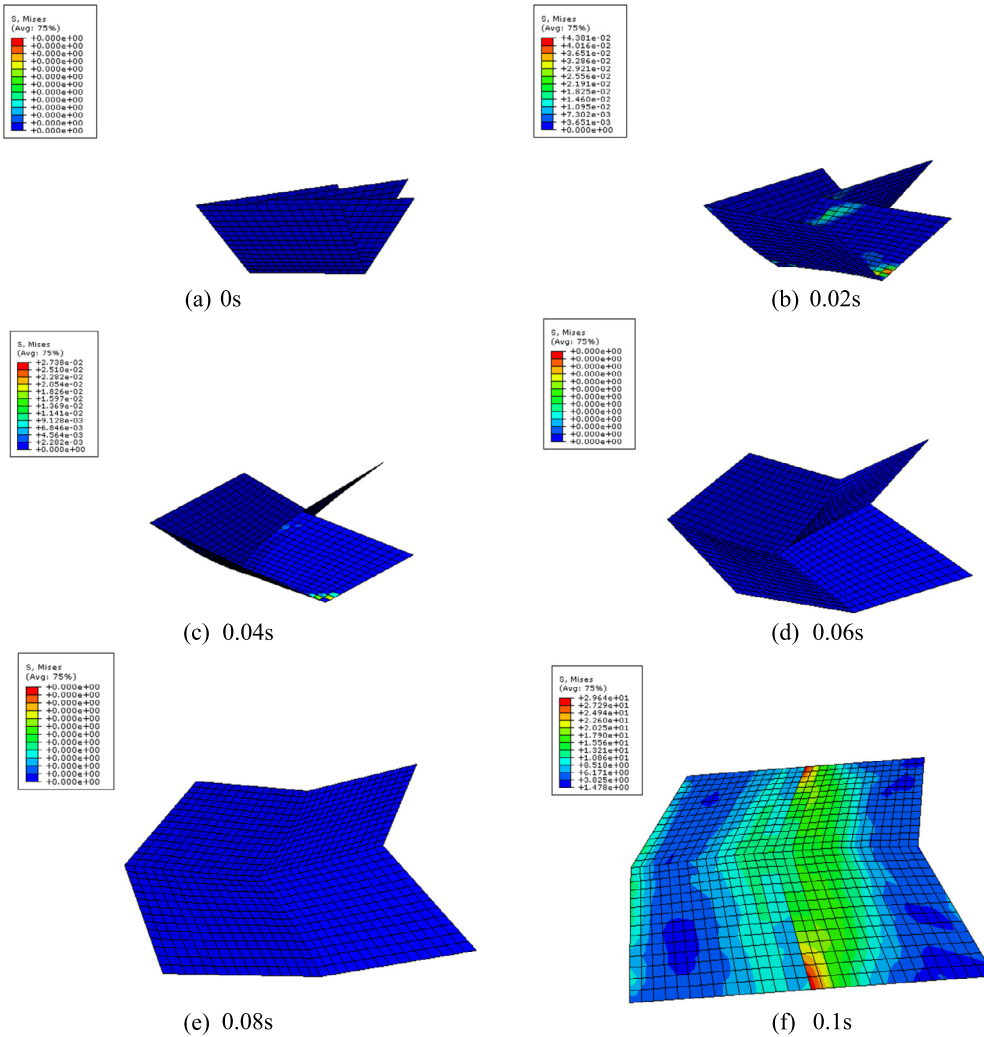


**Fig. 14.** The stress distribution during the motion (MPa).

**Table 4**  
Coordinates of nodes A, B and C (mm).

Node number	A	B	C
X-axis	2268.95	2268.95	2074.89
Y-axis	1253.19	1459.37	1459.37
Z-axis	99.977	99.977	99.977

maximum von Mises stress in the fully expanded state, were used to evaluate the results of numerical simulation.

As for the smoothness index, the ideal plane can be given by the coordinates of three corner nodes. Also the root means square of all nodes are defined as smoothness index of the membrane as

$$F = \sqrt{\frac{1}{n} \sum_{i=1}^n f_i^2} = \sqrt{\frac{f_1^2 + f_2^2 + \dots + f_n^2}{n}} \quad (6)$$

where  $n$  represents the number of nodes and  $f_i$  represents the distance between the node to the ideal plane defined by the coordinates of three nodes A, B and C as shown in Fig. 11.

For the configuration given in Fig. 13(f), the coordinates of three corner nodes are shown in Table 4. The equation of the plane defined by these three nodes is

$$40011.2908Z - 4000208.82 = 0 \quad (7)$$

Then the smoothness index is obtained as

$$F = \sqrt{\frac{1}{n} \sum_{i=1}^n f_i^2} = 3.421403 \text{ mm.} \quad (8)$$

It can also be found from Fig. 13 that the maximum Mises stress in the fully expanded state is 258.7 MPa. And there exists obvious stress concentration. The membrane cannot be unfolded fully, which leads to distortion occurs in the elements around the central points and stress concentration in the boundary elements. This can be due to the fact that there are few loading nodes, and the rest elements do not unfold fully. To validate this, the node loads were applied at all boundary nodes to ensure that all the boundaries are fully expanded. The stress distribution of the membrane during the motion is shown in Fig. 14.

It can be seen from Fig. 14 that the maximum Mises stress is 29.64 MPa. The smoothness index is 2.65 mm. It can be concluded that the results of loads applied on all boundary bounds are better than that imposed on one node. It indicates that multi-point loading is more appropriate. However, it is impossible to apply loads only on the corner nodes or all boundary nodes. In the next section, the influence of numbers of loading nodes will be studied.

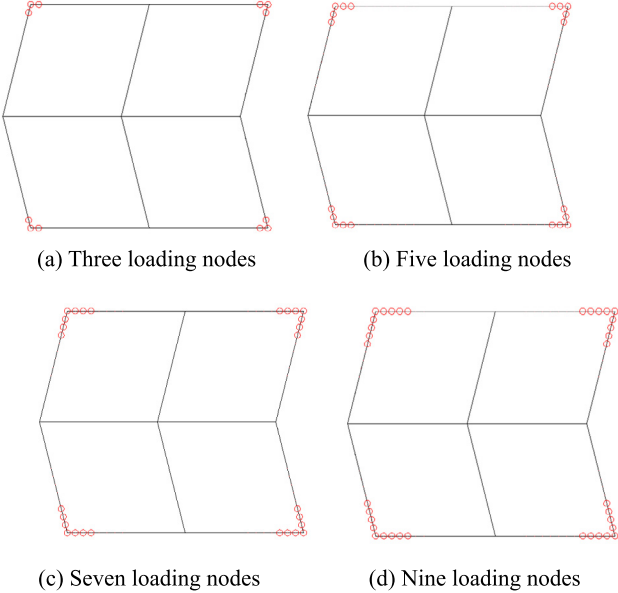


Fig. 15. Different types of loading nodes.

## 5. Parametric study

### 5.1. Number of loading nodes

Four loading types have been considered in this section, which are three, five, seven and nine loading nodes in one corner for each type as shown in Fig. 15. The stress contours in the final configuration with different numbers of loading nodes are given in Fig. 16. The maximum Mises stress and smoothness index are given in Table 5. The results under one loading node in one corner are also

**Table 5**  
Results with different numbers of loading nodes.

Numbers of loading nodes	Smoothness index $F$	Maximum mises stress (MPa)
1	3.42	258.7
3	3.38	200.7
5	3.23	90.68
7	3.24	66.52
9	2.51	75.63

shown in Table 5 for comparison. It can be found that the increase of numbers of the loading nodes can obviously reduce the maximum Mises stress in the fully expanded state, and the smoothness index is also lower and hence much better.

### 5.2. Loading time

The loading time may play an important role on the deployment performance of Miura-ori membranes. Effects of the loading time are investigated. It should be noted that when the loading time increases, the applied nodal velocity should have a corresponding decrease. The results are given in Table 6. It can be found that with the increase of loading time, the smoothness index and maximum Mises stress in fully expanded state show a decreasing trend. This may be because when the loading time is longer, the deployment process should have a pseudo-static behavior. When the loading time is 4 s, the deployment process of the membrane is shown in Fig. 17.

### 5.3. Boundary shape

When the loading time is 4 s, the results of the membrane with different numbers of loading nodes are given in Table 7. It can be found that the smoothness index and the maximum Mises

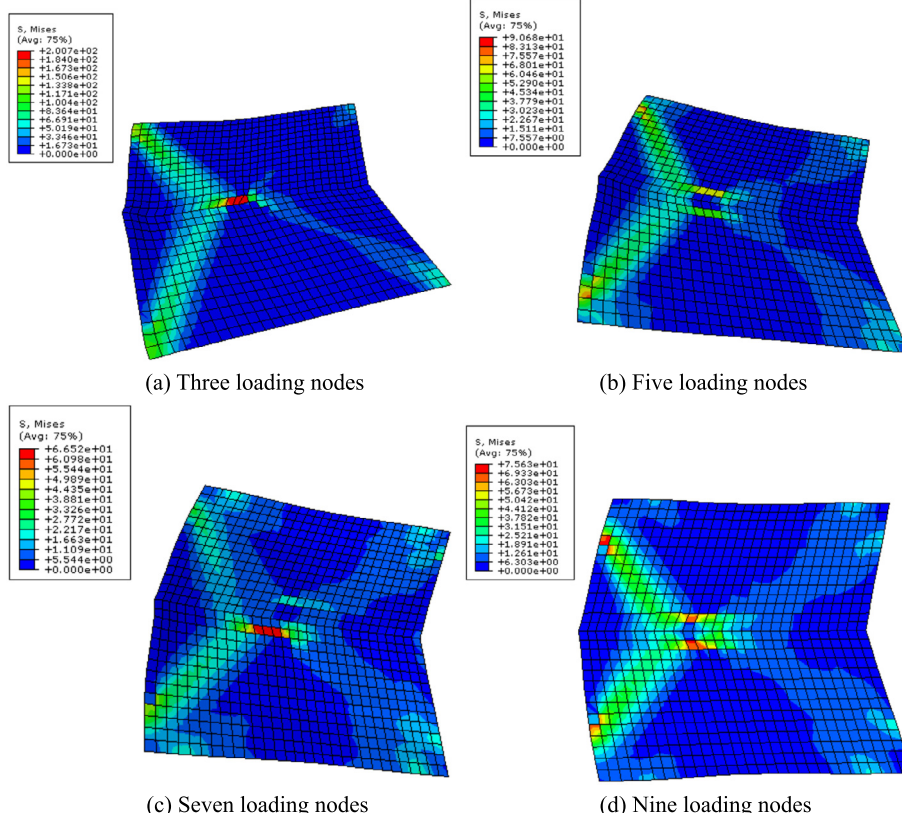
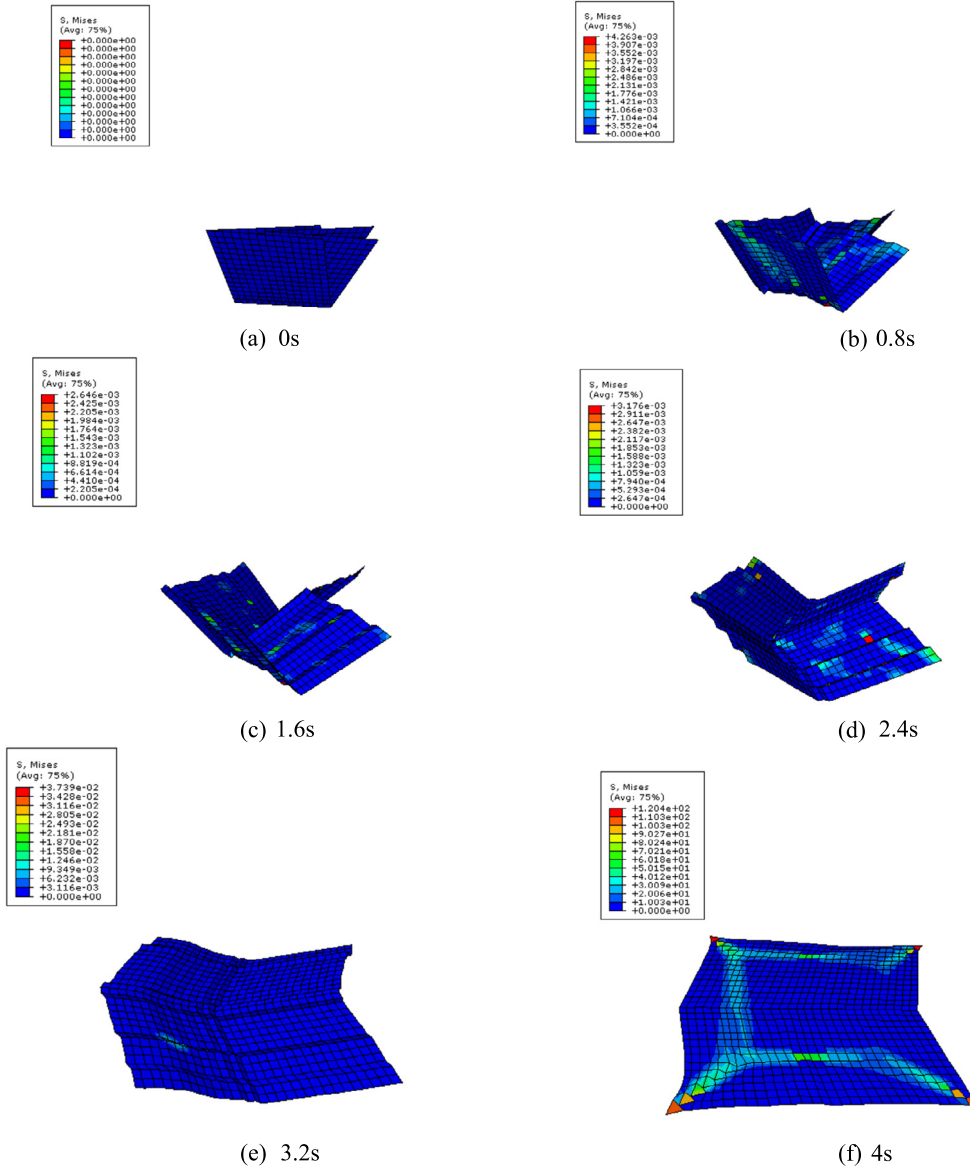


Fig. 16. The stress contour in the final configuration with different numbers of loading nodes (MPa).



**Fig. 17.** The deployment of membrane with the loading time of 4 s (MPa).

**Table 6**  
Results with different loading times.

Loading time	Smoothness index $F$	Maximum mises stress (MPa)
0.1s	3.42	258.7
1s	1.11	213.4
4s	0.04	120.4
8s	0.52	24.75

stress are almost increasing with the increase of number loading nodes. This is different from the previous conclusion of the influence of the numbers of loading nodes. The stress contour in the final configuration with different numbers of loading nodes is given in Fig. 18. It can be found that the stress concentration occurs at the half part with convex boundary. This might be for the reason that the membrane doesn't attain equilibrium state in the highly dynamic deployment process, which causes severe stress concentration.

A Miura-ori membrane with different boundary shapes, as shown in Fig. 19, is investigated to study its influence on the stress

**Table 7**  
Results with different numbers of loading nodes.

Numbers of loading nodes	Smoothness index $F$	Maximum mises stress (MPa)
3	0.59	89.25
5	1.46	124.1
7	1.39	151.2
9	1.23	150.9

in the deployed configuration. The size of the membrane is shown in Fig. 19(a) and the initial configuration in the fully compact configuration is given in Fig. 19(b).

The stress contour in the final configuration with different numbers of loading nodes is given in Fig. 20. It can be found that the maximum Mises stress decreases to 22.72 MPa, 36.09 MPa and 31.43 MPa for the 5, 7 and 9 loading numbers, respectively. The values are far lower than that of the original model, and there is no obvious stress concentration. Therefore, the effect of the boundary shape on the deployment behavior of the origami membrane is significant.

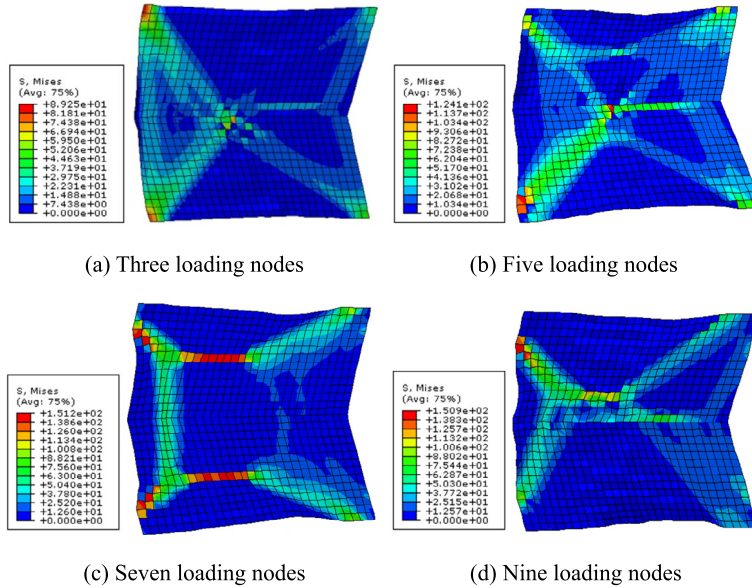


**Fig. 18.** The stress contour in the final configuration with different numbers of loading nodes (MPa).

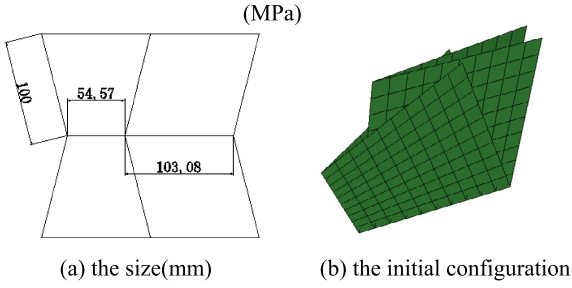


**Fig. 19.** A Miura-ori membrane with different boundary shapes.

## 6. Conclusions

The influence of the crease on the deployment of origami membrane is studied in this paper. The user material subroutine VUMAT is first adopted to revise the stress distribution of membrane elements to model the wrinkling of membranes, and it has been

shown reasonable by numerical simulations. The effective modulus of creased membrane is obtained by experiments.

In order to investigate the deploying process of membrane structure based on Miura origami, the smoothness index and the maximum Mises stress in the fully expanded state are used to evaluate the result of numerical simulation. Moreover, the effects of number of loading nodes, loading time and boundary shape are also studied. It can be found that the increase of the loading nodes can effectively reduce the smoothness index and the maximum Mises stress in the fully expanded state. By increasing the loading time, the smoothness index becomes lower. Stress concentration may occur under the condition of multi-node loading. But the model with two concave boundaries can solve this problem. Therefore, the shape of membrane is important to the deployment of Miura-ori membrane. The form-finding study should be carried out in the future to satisfy the equilibrium condition of the membrane when it is used for the deployment of a solar sail [12].

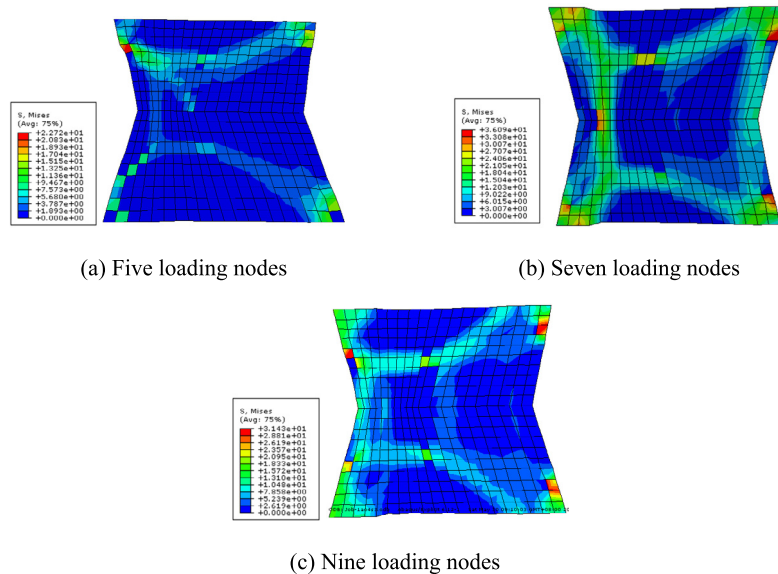


**Fig. 20.** Results of different boundary shape (MPa).

## Conflict of interest statement

Authors have no conflict of interest.

## Acknowledgements

The work presented in this article was supported by the National Natural Science Foundation of China (Grant No. 51308106, No. 51578133), a Project Funded by the Priority Academic Program Development of Jiangsu Higher Education Institutions, and the Excellent Young Teachers Program of Southeast University. A preliminary version of this article was presented at the ASME 2016 International Design and Engineering Technical Conferences & Computers and Information in Engineering Conference. Authors also thank the anonymous reviewers for their valuable comments and thoughtful suggestions which improved the quality of the presented work.

## References

- [1] C. Liu, Y. Shi, Comprehensive structural analysis and optimization of the electrostatic forming membrane reflector deployable antenna, *Aerosp. Sci. Technol.* 53 (2016) 267–279.
- [2] Q. Tao, C. Wang, Z. Xue, Z. Xie, H. Tan, Wrinkling and collapse of mesh reinforced membrane inflated beam under bending, *Acta Astronaut.* 128 (2016) 551–559.
- [3] D.M. Murphy, Validation of a scalable solar sailcraft system, *J. Spacecr. Rockets* 44 (4) (2007) 797–808.
- [4] X. Hu, S. Gong, Flexibility influence on passive stability of a spinning solar sail, *Aerosp. Sci. Technol.* 58 (2016) 60–70.
- [5] M. Schenk, A.D. Viquerat, K.A. Seffen, S.D. Guest, Review of inflatable booms for deployable space structures: packing and rigidization, *J. Spacecr. Rockets* 51 (3) (2014) 762–778.
- [6] Y. Chen, R. Peng, Z. You, Origami of thick panels, *Science* 349 (6246) (2015) 396–400.
- [7] J.G. Cai, X.W. Deng, Y.X. Xu, J. Feng, Geometry and motion analysis of origami-based deployable shelter structures, *J. Struct. Eng. ASCE* 141 (10) (2015) 06015001.
- [8] J.G. Cai, X.W. Deng, J. Feng, Y. Zhou, Geometric design and mechanical behavior of a deployable cylinder with Miura origami, *Smart Mater. Struct.* 24 (2015) 125031.
- [9] J.G. Cai, X.W. Deng, Y.X. Xu, J. Feng, Motion analysis of a foldable barrel vault based on regular and irregular Yoshimura origami, *J. Mech. Robot. ASME* 8 (2) (2016) 021017.
- [10] K. Miura, Method of packaging and deployment of large membranes in space, in: Proceedings of 31st Congress of International Astronautics Federation (IAF-80-A31), Tokyo, Japan, 1980, pp. 1–10.
- [11] K. Miura, M. Natori, 2-D array experiment on board a space flyer unit, *Space Sol. Power Rev.* 5 (4) (1985) 345–356.
- [12] G.C. Horner, M.D. Elliot, A fabrication and deployment approach for a Miura-Ori solar sail model, in: 43rd AIAA/ASME/ASCE/AHS/AHS Structures, Structural Dynamics and Materials Conference, 2002, AIAA Paper 2002-1708.
- [13] X.F. Wang, Q.S. Yang, S.S. Law, Wrinkled membrane element based on the wrinkling potential, *Int. J. Solids Struct.* 51 (21/22) (2014) 3532–3548.
- [14] B. Fu, F. Eke, Further investigation of the body torques on a square solar sail due to the displacement of the sail attachment points, *Aerosp. Sci. Technol.* 50 (2016) 281–294.
- [15] X.W. Deng, Clefited Equilibrium Shapes of Superpressure Balloon Structures, California Institute of Technology, 2012.
- [16] X. Wang, J. Ma, S.S. Law, Q. Yang, Numerical analysis of wrinkle-influencing factors of thin membranes, *Int. J. Solids Struct.* 97 (2016) 458–474.
- [17] Y. Zhang, F. Gao, S. Zhang, J. Hao, Electrode grouping optimization of electrostatic forming membrane reflector antennas, *Aerosp. Sci. Technol.* 41 (2015) 158–166.
- [18] I.M. Ward, Mechanical Properties of Solid Polymers, 2nd edition, John Wiley & Sons, 1985.
- [19] E. Reissner, On tension field theory, in: Proceedings Fifth International Congress of Applied Mechanics, 1938, pp. 88–92.
- [20] C.G. Wang, H.F. Tan, X.W. Du, Z.M. Wan, Wrinkling prediction of rectangular shell-membrane under transverse in-plane displacement, *Int. J. Solids Struct.* 44 (2007) 6507–6516.
- [21] C.G. Wang, L. Lan, Y.P. Liu, L. Zhang, H.F. Tan, A numerical algorithm for eliminating the singular stiffness matrix of membrane wrinkling, in: 54th AIAA/ASME/ASCE/AHS/ASC Structures, Structural Dynamics, and Materials Conference, April 8–11, 2013, Boston, Massachusetts, AIAA 2013-1930.
- [22] M. Stein, J.M. Hedgepeth, Analysis of Partly Wrinkled Membranes, NASA Technical Note TN D-813, Langley Research Center, Langley Field, VA, 1961.
- [23] R.K. Miller, J.M. Hedgepeth, An algorithm for finite element analysis of partly wrinkled membranes, *AIAA J.* 20 (1982) 1761–1763.
- [24] A. Patil, A. Nordmark, A. Eriksson, Instabilities of wrinkled membranes with pressure loadings, *J. Mech. Phys. Solids* 94 (2016) 298–315.
- [25] A. Patil, A. Nordmark, A. Eriksson, Wrinkling of cylindrical membranes with non-uniform thickness, *Eur. J. Mech. A, Solids* 54 (2015) 1–10.
- [26] A. Gough, N.M.A. Hossain, C.H. Jenkins, J. Blandino, A. Hendricks, Experimental and numerical study of creased membranes, in: Proc. of 46th AIAA/ASME/ASCE/AHS/ASC Structures, Structural Dynamics, and Materials Conference, 18–21 Apr. 2005, Austin, Texas, AIAA 2005-1976.
- [27] K. Woo, K. Nandukar, C.H. Jenkins, Effective modulus of creased thin membranes, *J. Spacecr. Rockets* 45 (1) (2008) 19–26.
- [28] K. Woo, C.H. Jenkins, Analysis of wrinkling behavior of creased thin membranes, in: Proc. of 48th AIAA/ASME/ASCE/AHS/ASC Structures, Structural Dynamics, and Materials Conference, 23–26 April, 2007, Honolulu, HI, AIAA 2007-1818.
- [29] K. Woo, C.H. Jenkins, Thickness effect on wrinkle–crease interaction for thin sheets, in: Proc. of 49th AIAA/ASME/ASCE/AHS/ASC Structures, Structural Dynamics, and Materials Conference, 7–10 April, 2008, Schaumburg, IL, AIAA 2008-2136.
- [30] K. Woo, C.H. Jenkins, Effect of crease orientation on wrinkle–crease interaction in thin sheets, in: Proc. of 50th AIAA/ASME/ASCE/AHS/ASC Structures, Structural Dynamics, and Materials Conference, 4–7 May, 2009, Palm Springs, California, AIAA 2009-2162.
- [31] K. Woo, C.H. Jenkins, Analysis of crease–wrinkle interaction for thin sheets, *J. Mech. Sci. Technol.* 26 (3) (2012) 905–916.
- [32] C.G. Wang, H.F. Tan, X.D. He, Wrinkle–crease interaction behavior simulation of a rectangular membrane under shearing, *Acta Mech. Sin.* 27 (4) (2011) 550–558.
- [33] A. Papa, S. Pellegrino, Systematically creased thin-film membrane structures, *J. Spacecr. Rockets* 45 (1) (2008) 10–18.
- [34] A.L. Adler, Finite Element Approaches for Static and Dynamic Analysis of Partially Wrinkled Membrane Structures, University of Colorado, 2000.